AGU PUBLICATIONS

Geophysical Research Letters

RESEARCH LETTER
10.1002/2014GL060782

Key Points:
- Slip rates of Gyaring Co Fault are determined from lacustrine shoreline offset
- The average slip rate is 2.2–4.5 mm/yr during the latter half of Holocene
- The slip of this fault is similar to other strike-slip faults in interior Tibet

Supporting Information:
- Readme
- Figure S1
- Figure S2
- Figure S3
- Figure S4
- Figure S5
- Figure S6
- Table S1
- Table S2
- Table S3

Correspondence to:
X. Shi,
xuhua.shi@gmail.com

Citation:
Shi, X., E. Kirby, H. Lu, R. Robinson, K. P. Furlong, and E. Wang (2014), Holocene slip rate along the Gyaring Co Fault, central Tibet, *Geophys. Res. Lett.*, *41*, 5829–5837, doi:10.1002/2014GL060782.

Received 6 JUN 2014
Accepted 2 AUG 2014
Accepted article online 7 AUG 2014
Published online 20 AUG 2014

Holocene slip rate along the Gyaring Co Fault, central Tibet

Xuhua Shi[1], Eric Kirby[2], Haijian Lu[3], Ruth Robinson[4], Kevin P. Furlong[1], and Erchie Wang[5]

[1]Department of Geosciences, Pennsylvania State University, University Park, Pennsylvania, USA, [2]College of Earth, Ocean, and Atmospheric Sciences, Oregon State University, Corvallis, Oregon, USA, [3]Institute of Geology, Chinese Academy of Geological Sciences, Beijing, China, [4]Department of Earth and Environmental Sciences, University of St Andrews, St. Andrews, UK, [5]Institute of Geology and Geophysics, Chinese Academy of Sciences, Beijing, China

Abstract Although geodetic measurements of interseismic deformation in interior Tibet suggest slow strain accumulation, active slip along the right-lateral Gyaring Co Fault is suggested to be between 8 and 21 mm/yr. Reliable geologic constraints on the slip rate along this fault are sparse. Here we document 12 ± 2 m of right-lateral displacement of lacustrine shorelines across the Gyaring Co Fault. Optically stimulated luminescence ages of the shorelines are tightly clustered between 4.1 and 4.4 ka. These data require an average slip rate of 2.2–3.2 mm/yr along the central Gyaring Co Fault during the latter half of the Holocene. Consideration of seismic cycle effects allows the possibility of slightly higher average slip rates, up to 2.2–4.5 mm/yr. Overall, our results suggest that the slip rate along the Gyaring Co Fault is similar to other strike-slip faults in interior Tibet, supporting the notion that active deformation in this region is distributed among numerous, slowly moving faults.

1. Introduction

Intracontinental deformation within the Himalayan-Tibetan orogen presently accommodates ~40 mm/yr of north-south convergence between India and Eurasia [*Paul et al.*, 2001; *Wang et al.*, 2001]. Approximately half of this convergence is accommodated by shortening across the Himalaya [*Ader et al.*, 2012; *Bettinelli et al.*, 2006], and the remainder is distributed northward throughout the adjacent Eurasian lithosphere. Whether active deformation is primarily localized along major strike-slip fault systems (Figure 1) [*Avouac and Tapponnier*, 1993; *Peltzer and Tapponnier*, 1988] or occurs as distributed strain within the interior of the plateau [*England and Houseman*, 1986] has been a point of debate. The former hypothesis implies that rapid slip along the major strike-slip faults absorbs a large fraction of the total convergence [e.g., *Chevalier et al.*, 2005a; *Mériaux et al.*, 2004], whereas the latter hypothesis implies relatively low displacement rates [e.g., *Brown et al.*, 2002; *Cowgill et al.*, 2009] along the numerous active faults throughout Tibet.

This fundamental difference in deformational behavior in Tibet has received extensive attention in recent years. A preponderance of evidence now suggests that many of these faults have slip rates on the order of ~1 cm/yr when averaged over the late Pleistocene-Holocene timescales. Along the Altyn Tagh Fault, slip rates determined at numerous sites indicate average rates of ~10 mm/yr (Figure 1) [*Chen et al.*, 2012, 2013; *Cowgill*, 2007; *Cowgill et al.*, 2009; *Gold et al.*, 2009; *Washburn et al.*, 2001; *Zhang et al.*, 2007]. Studies along the central Kunlun Fault [*Li et al.*, 2005; *Van der Woerd et al.*, 1998, 2000, 2002] indicate slip rates of ~8–10 mm/yr, and the Karakorum Fault appears to have slip rates between ~5 and 8 mm/yr [*Brown et al.*, 2005, 2002; *Chevalier et al.*, 2012, 2005a, 2005b, 2011]. These modest slip rates determined from offset geomorphic markers are similar to those inferred from space geodesy [e.g., *Bendick et al.*, 2000; *Elliott et al.*, 2008; *He et al.*, 2013; *Wright et al.*, 2004]. Although it has been suggested that some faults may exhibit temporal variations in slip rate [e.g., *Chevalier et al.*, 2005a], most of the data appear to be consistent with a relatively constant slip rate through time [e.g., *Gold et al.*, 2009; *He et al.*, 2013]. Spatial variations of slip rates along some of these major structures [*Harkins and Kirby*, 2008; *Harkins et al.*, 2010; *Kirby et al.*, 2007; *Zhang et al.*, 2007] are associated with distributed deformation throughout the plateau [*Kirby and Harkins*, 2013]. These studies make a strong case that the degree of strain localization along major strike-slip faults largely reflects heterogeneity in the strength of Tibetan crust/lithosphere [e.g., *England and Houseman*, 1985; *Molnar and Dayem*, 2010].

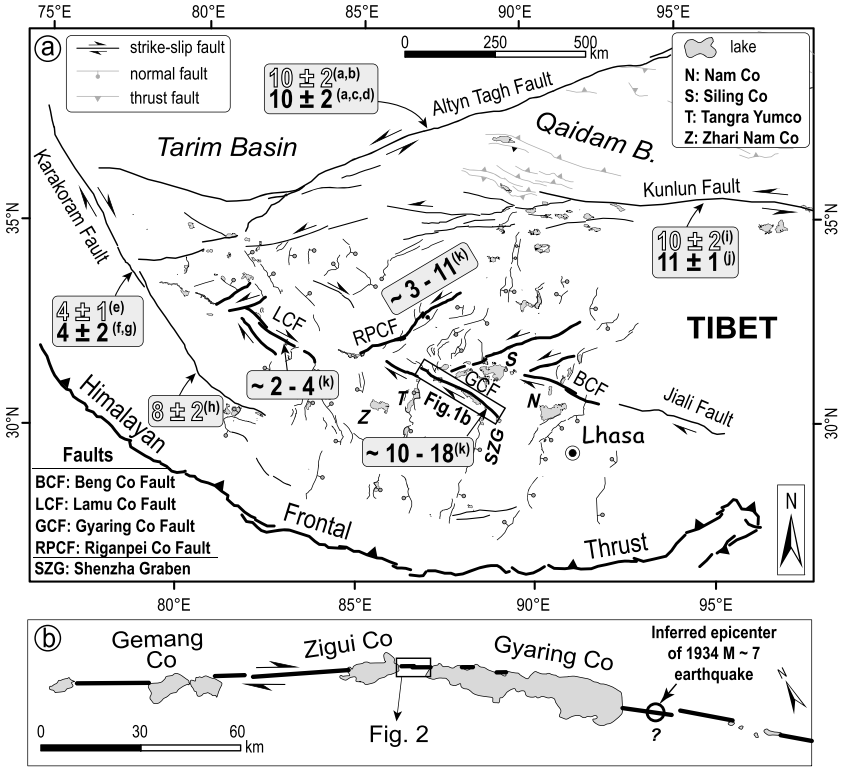

Figure 1. (a) The tectonic setting of the interior Tibetan Plateau. The fault systems are adopted from *Taylor and Yin* [2009]. Bold lines represent fault traces of conjugate strike-slip fault systems in central Tibet [*Taylor et al*., 2003]. Black numbers in shaded boxes denote geodetically derived rates, and white numbers for geologically derived long-term rates. References: *Zhang et al*. [2007] (a), *Cowgill et al*. [2009] (b), *Bendick et al*. [2000] (c), *Shen et al*. [2001] (d), *Brown et al*. [2002] (e), *Chevalier et al*. [2012] (f), *Wright et al*. [2004] (g), *Jade et al*. [2004] (h), *Van der Woerd et al*. [2000] (i), *Zhang et al*. [2004] (j), and *Taylor and Peltzer* [2006] (k). (b) The detailed view of the GCF segments. The open circle indicates the possible location for the 1934 Shenzha earthquake.

Within the interior of the Tibetan Plateau, geodetic and geologic observations suggest that active deformation is accomplished along a network of conjugate strike-slip fault systems [*Taylor et al*., 2003] and associated N-S trending rift systems (Figure 1). Geodetic data suggest that rates of E-W extension are quite low, ranging from $<$1 to 4 mm/yr [*Chen et al*., 2004b; *Elliott et al*., 2008; *Gan et al*., 2007; *Liang et al*., 2013]. This is consistent with relatively slow slip rates determined along graben-bounding normal faults [*Armijo et al*., 1986; *Blisniuk and Sharp*, 2003; *Molnar and Lyon-Caen*, 1989; *Yin et al*., 1999]. Likewise, slip rates along NW-SE and NE-SW striking faults inferred from geodetic data also appear to be modest: (1) interferometric synthetic aperture radar (InSAR) results indicate left-lateral slip rates $<$~6 mm/yr of the Riganpei Co Fault [*Taylor and Peltzer*, 2006] and (2) similar observations across the Lamu Co, Beng Co, and Dongqiao Faults suggest slip rates of 1–3 mm/yr [*Garthwaite et al*., 2013; *Taylor and Peltzer*, 2006]. Although early workers suggested rapid slip along a through-going fault system (the "Karakorum-Jiali fault zone" [*Armijo et al*., 1989, 1986]), the present-day strain field appears to be characterized by slow N-S shortening and E-W extension accommodated along a distributed array of conjugate strike-slip fault systems [*Chen et al*., 2004a; *Taylor et al*., 2003].

An exception may occur along the dextral Gyaring Co Fault (GCF, Figure 1), where slip rates are thought to be high [*Armijo et al*., 1989; *Taylor and Peltzer*, 2006]. The GCF represents one of the primary conjugate faults in the region [*Taylor et al*., 2003], and *Armijo et al*. [1989] suggest that it has sustained Holocene slip rates of ~15 mm/yr on the basis of fresh scarps and displaced landforms. Although these geomorphic features were not dated, analysis of stacked InSAR data appears to confirm rapid strain accumulation across the fault system, with slip rates between ~8 and 21 mm/yr [*Taylor and Peltzer*, 2006]. Because there are no direct constraints on the average geologic slip rate of the GCF, the significance of these high apparent rates remains uncertain. Here we place quantitative bounds on the Holocene slip rate of the GCF by reconstructing displaced lacustrine shorelines around Zigui Co ("Co" means lake in Tibetan), a lake immediately northwest of Gyaring Co (Figure 1).

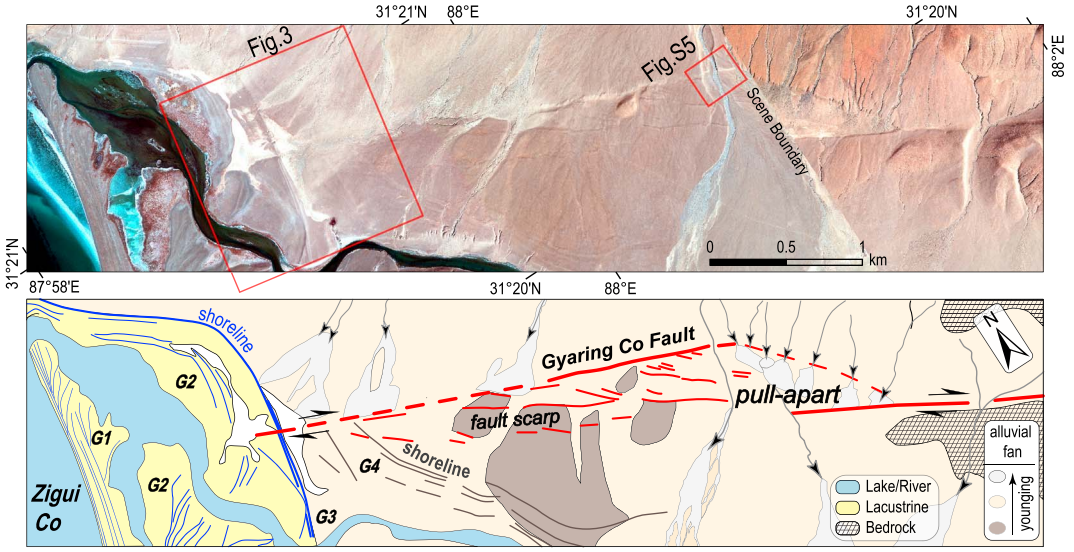

Figure 2. GeoEye (top) imagery and (bottom) sketch map showing fault displacements and scarps of the central segment of the GCF, four groups of shorelines, and other geological units at the southeastern margin of Zigui Co.

2. Background

The GCF (Figure 1a) is a WNW striking fault that extends along the northern shore of Gyaring Co (Figure 1b) and forms the northern boundary of several major N-S striking grabens (Figure 1). The fault extends ~250 km and consists of several segments exposed between major lakes that cover the fault trace (Figure 1b). The fault trace is prominent and marked by fresh scarps that displace alluvial fans and fan terraces, channels, and lacustrine shorelines in a right-lateral sense [*Armijo et al*., 1989; *Taylor and Peltzer*, 2006].

The GCF has been proposed to be a component of a regional shear zone (the "Karakorum-Jiali fault zone") that was suggested to act in concert with the left-lateral Altyn Tagh and Kunlun Faults in accommodating eastward extrusion of northern Tibet [*Armijo et al*., 1989]. Other studies consider the GCF one among a network of conjugate fault systems in central Tibet [*Taylor et al*., 2003; *Yin and Taylor*, 2011]. The fault appears to merge toward the northwest with the NE striking, left-lateral Riganpei Co Fault, and toward the southeast, the GCF appears to be kinematically linked with the Shenzha rift system (Figure 1).

Recent analysis of stacked InSAR interferograms across the northern segment of this fault suggests relatively rapid slip rates (~8–21 mm/yr) [*Taylor and Peltzer*, 2006], similar to the inference of ~15 mm/yr from displaced geomorphic features [*Armijo et al*., 1989]. These authors argued that rapid slip along the fault is consistent with the occurrence of an $M \sim 7$ earthquake that occurred in 1934 in the general vicinity of the Shenzha rift [*Armijo et al*., 1989]. The location of the 1934 event is still debated, whether this event occurred along the southeastern branch of the GCF [*Armijo et al*., 1989] or was perhaps related to the normal faulting in the Shenzha graben [*Wu et al*., 1990] is unknown. This uncertainty, coupled with the absence of quantitative estimates of the Holocene slip rate along the GCF make it difficult to ascertain the significance of rapid slip inferred from geodetic data [*Taylor and Peltzer*, 2006].

3. Holocene Slip Rate Along the Gyaring Co Fault

3.1. Zigui Co Fault Site

Our study site is located along the central segment of the fault system between Gyaring Co and Zigui Co (Figure 1b). Approximately 5 km east of the present-day shoreline of Zigui Co, the active fault trace is marked by two primary strands that comprise a right step in the fault system (Figure 2). The presence of the scarps and the rhomboid topographic depression formed between the fault strands, confirm this as an extensional step, compatible with right-lateral displacement along the fault (Figure 2). The northern margin of the pull-apart is marked by a prominent south-facing scarp that separates dissected alluvial fans from the basin

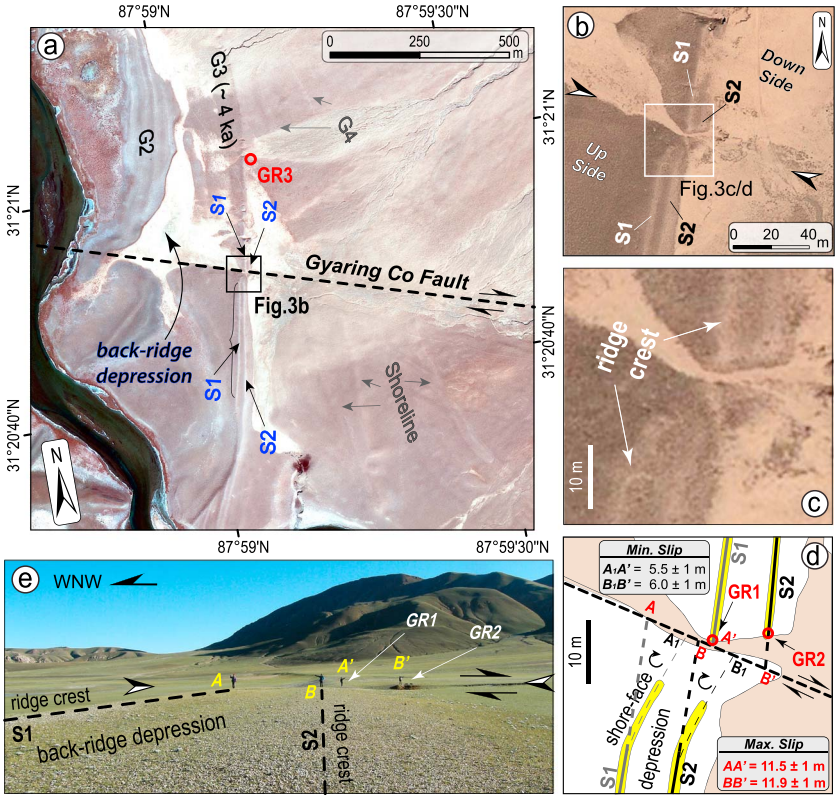

Figure 3. (a) GeoEye imagery showing shoreline groups G2–G4 where the G3 shorelines were displaced. The bracket south of the fault represents straight parts of the shorelines (~350–400 m). (b) Overview of the fault displacement on the G3 shorelines. Arrows point to the fault trace. (c) Detailed view of fault displacements in the imagery. (d) Sketch of reconstruction of fault displacements. Yellow stripes denote ridge crests shown in Figure 3c. Tan-colored area shows the back-ridge depression. (e) Field photo looking to the north that shows shoreline offset.

(Figure 2). Near the western end of the pull-apart, this fault strand displaces several younger generations of alluvial fans and inset fan-terrace surfaces (Figure 2). Toward the west, the northern fault strand appears to carry most of the displacement; near the margin of Zigui Co, scarps along the southern fault strand are small and discontinuous (Figure 2).

We observed four groups (G1–G4) of relict shorelines to the southeast of Zigui Co (Figure 2). Shoreline groups G3 and G4 are interpreted to mark former, higher levels of Zigui Co. The highest of these features are wave-cut scarps developed discontinuously along the alluvial fans south of the GCF. These wave-cut scarps trend WNW, along the slope of the alluvial apron (G4 in Figure 2b). They appear to be significantly degraded, with rounded crests and extensive gully networks developed along the risers. The lower set of shorelines is marked by prominent beach ridges and spits, composed of beach and shoreface deposits during a high lake stage. Two primary ridges form an arcuate trace that trends N-S along the eastern margin of the lake (G3 in Figure 2). In contrast to the higher shorelines, these features are fresh, undissected, and act as barriers to modern drainage; fine-grained sand and silt are ponded to the east of the beach ridges (Figure 2). To the west of these shoreline groups are lower shorelines and beach ridges associated with the modern level of Zigui Co (G2 and G1 in Figure 2).

We focus our study on the G3 shoreline group for two reasons. First, this group forms a sharp linear marker that intersects the GCF at a high angle (Figure 3). South of the fault, the beach ridges are remarkably straight, extending south from the scarp for several hundred meters. North of the fault, the beach ridges again extend for several hundred meters and then merge into a wave-cut scarp developed in older alluvium (Figure 3). The extensive linear character of the ridges, absent embayments and cusps, and their near-orthogonal orientation with respect to the fault trace make these ideal markers to reconstruct displacement along the GCF. Moreover, because the G3 shorelines are depositional features, their ages are not subject to some of the

ambiguity associated with fluvial terrace risers [*Cowgill*, 2007; *Harkins and Kirby*, 2008]; the age of deposition of the shoreline places a direct constraint on the slip rate since the shoreline was established.

The beach ridges exhibit cross-sectional topography typical of constructional shorelines: a primary ridge with a flat top (~1–2 m wide, light-colored stripes in Figure 3a), a lakeward front scarp and a subtle depression on the landward side (light-colored region in Figure 3a). Pits excavated in the beach ridges reveal distinct stratigraphy of these deposits consisting of 5–10 cm thick layers of rounded, well-sorted gravels, intercalated with thin sandy layers (Figures S1 and S2 in the supporting information). In contrast, the back-ridge depressions (Figure 3a) are filled with coarse-to-medium-grained eolian sands (Figure S3) interbedded with alluvial sands and gravels. In both depositional settings, we determined the shoreline ages using optically stimulated luminescence (OSL) dating.

3.2. Reconstructing Fault Slip

Using GeoEye satellite images (nominal resolution ~0.5 m), we project the center lines (Figure 3d) of the ridge flats (~1–2 m wide) (Figures 3e and S4) into the fault trace. We also surveyed the position of these intersections along the fault with a measuring tape in the field. Both beach ridges exhibit a ~30° clockwise bend in their traces as they approach the fault (Figures 3c and 3d). Because the shorelines are nearly linear for $>$350 m north and south of the fault trace and because those to the north of the fault are consistently displaced to the east relative to the southern shorelines, we argue that this bend must reflect near-fault deformation. We do not believe that it was an embayment in the shoreline coincident with the trace of the fault. We believe that the most likely interpretation is that the bends are "drag folds" related to dextral shear in the shallow alluvium [*Shelef and Oskin*, 2010], but we acknowledge the possibility that they may reflect postrupture erosional modification of the intersection between the shoreline and the fault scarp during lake-level oscillations at the G3 highstand.

Projecting the linear crest of the beach ridges in the field yields estimates of displacement along the GCF of 11.5 m along shoreline 1 (S1) and 11.9 m along shoreline 2 (S2) (Figure 3d). Given that the strike separation was measured manually by tape and that the width of the ridge flats is ~1–2 m, we assign an uncertainty of 1 m (or, half the width of the ridge flats) for all measurements. We measured the offsets for both shorelines in the imagery using the same approach of digitizing the center line; this analysis yields similar displacements of ~13 ± 1 m. Thus, our best estimate of lateral slip along the GCF is ~12 ± 2 m. In addition to the strike-slip component, the GCF also exhibits minor vertical separation at this site, with the southern side of the fault 0.5–1 m higher than the northern side (Figure S4).

Importantly, we do not find evidence for displacement of the youngest alluvial and lacustrine features along this segment of the GCF. Although the geometry of G2 shorelines is suggestive that they have been cut by the fault (Figure 2), the fault trace is buried by recent alluvium at this location. Moreover, the curvilinear traces of the G2 shoreline features (Figure 2), in contrast to the straight ridges of G3 shorelines, make any reconstruction highly uncertain. It is clear, however, that the G1 shoreline, immediately adjacent to the modern lake margin, is not displaced across the fault (Figure 2). Thus, these features provide a lower bound for the most recent surface-rupturing event along the fault. Similarly, we observe scarps developed along the fault trace in relatively young alluvial terraces bounding the northwestern margin of the pull-apart basin (Figures 2 and S5). The youngest of these terraces (T1 in Figure S5) is not cut by the fault. Unfortunately, we were unable to obtain appropriate material for dating either the G1 shorelines or this youngest alluvial surface.

3.3. Shoreline Chronology and Fault Slip Rate

We determined ages of the G3 shorelines by OSL dating of medium-to-fine-grained sands in the shoreline deposits. Three samples were collected: two (GR1 and GR2 in Figure 3b) from sand layers interbedded with the beach gravel layers within pits (Figure S1) in shorelines S1 and S2 and another (GR3 in Figure 3a) from the eolian sand deposits in the depression east of shoreline S1. The presence of medium-grained sands in the upper 1–2 m of the soil pits (GR1 and GR2) suggest that burial ages of the OSL samples should reflect the time since final aggradation of S1 and S2 shorelines. Samples were prepared using standard OSL procedures and analyzed using the single aliquot regenerative dose protocol and small aliquots (see methods in the supporting information) [*Murray and Wintle*, 2000].

Our results suggest that the shorelines S1 and S2 were deposited at 4.1 ± 0.1 ka and 4.1 ± 0.3 ka, respectively (Table S2). The age for sample GR3 is similar, 4.4 ± 0.3 ka (Table S2), suggesting that deposition of the eolian sands appears to have been synchronous with the development of the beach ridges. These tightly clustered ages of the three samples, regardless of the variation in burial depth, yield estimates of the average slip rate during the

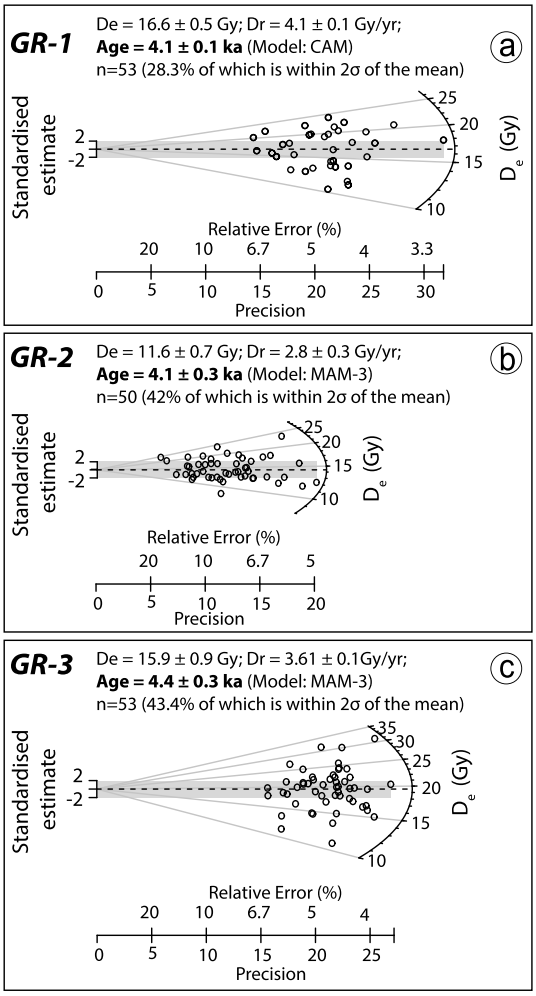

Figure 4. Radial plots showing the distribution of equivalent dose (De) for each sample. Gray shading shows the aliquots used for modeling OSL ages. Dr is the dose rate; *n* is the number of aliquots analyzed for each sample. Age model description is provided in the supporting information.

latter part of the Holocene that range from 2.2 to 3.2 mm/yr. Thus, our results require relatively modest slip rates along the GCF during the Holocene time.

4. Discussions and Implications

Our findings imply a large discrepancy between our Holocene slip rate (2.2–3.2 mm/yr) and geodetically determined slip rate (8–21 mm/yr) [e.g., *Taylor and Peltzer*, 2006] along the GCF. It is increasingly recognized that secular variation in fault slip [e.g., *Wallace*, 1987], potentially associated with earthquake clusters [e.g., *Rockwell et al.*, 2000], may influence the time-averaged slip rate along intracontinental faults [*Chevalier et al.*, 2005a; *Rittase et al.*, 2014]. To evaluate the possible contributions of earthquake histories to our estimate of slip rate, we consider an alternative scenario of an earthquake event to occur in the near future. We consider it unlikely that the entire 11–12 m of displacement accrued in a single earthquake. Maximum coseismic slip during large strike-slip events—the M_w 7.6 Manyi earthquake in 1997 (~7 m) [*Peltzer et al.*, 1999], the M_w 7.9 Kokoxili earthquake in 2001 (~7–8 m) [*Xu et al.*, 2006], the M_s 7.9 Fuyun earthquake in 1931 (~5–7 m) [*Klinger et al.*, 2011], and even the M_w 7.9 Fort Tejon earthquake of 1857 along the San Andreas Fault (~5–6 m) [*Zielke et al.*, 2010]—were all on the order of ~6 m. Thus, it seems reasonable that the total displacement of ~12 ± 2 m at the Zigui Co site reflects at least two events and perhaps more (if characteristic earthquakes had magnitudes M_w of 6–7) [*Stirling et al.*, 2002]. Thus, our slip rates probably represent a reasonable average over at least two seismic cycles.

Although we do not have direct constraints on the age of the youngest shoreline (G1), the absence of scarps cutting these features implies that the 1934 M ~ 7 Shenzha earthquake did not contribute to displacement of the G3 shorelines. Because the epicenter of the 1934 event is located ~70 km southeast of our site, this may reflect termination of the rupture farther east along the GCF. Alternatively, it may be consistent with the suggestion that the 1934 event occurred within the Shenzha graben [*Wu et al.*, 1990]. Regardless, these data suggest that our slip estimate is not likely influenced by a relatively recent, historic or prehistoric, earthquake. This forces us to consider the maximum slip rate allowable by our data. If we presume that displacement along this segment of the fault accrued during two events with slip of ~6 m, then it is possible that an event of similar size in the near future would lead to a total displacement of ~18 m. Thus, even if the fault is extremely late in the earthquake cycle, our data would imply that the average slip rate during the latter half of the Holocene could be no greater than 3.6–4.5 mm/yr. Thus, we argue that the maximum allowable range of slip rates, including potential seismic cycle effects, is 2.2–4.5 mm/yr. This further implies that the large differences between our determination of fault slip rate and the geodetic data are probably not an artifact of a limited rupture history at our site. Whether these differences reflect the choice of parameters in the fault model

[*Taylor and Peltzer*, 2006] or temporal variations in the slip rate remains unclear. But if the geodetic data are a complete reflection of strain accumulation along the GCF, it would appear that this fault is being loaded at a far greater rate than strain has been released. Our results highlight the need for additional constraints on slip rate farther back in time to evaluate the potential for secular variations in displacement.

From a regional perspective, our slip rate of 2.2–4.5 mm/yr along the GCF during the Holocene is consistent with slip rates determined along several other faults in central western Tibet. Geodetic measurements of interseismic strain determined from InSAR suggest that many of the conjugate strike-slip faults are moving at modest rates (Figure 1): (1) the Lamu Co Fault in western Tibet (~2–4 mm/yr) [*Taylor and Peltzer*, 2006], (2) the Riganpei Co Fault (~3–11 mm/yr) [*Taylor and Peltzer*, 2006], and (3) the Beng Co Fault (~1–4 mm/yr) [*Garthwaite et al*., 2013]. Although we do not directly address the question of whether the Karakorum-Jiali fault zone is a continuous structural feature during the Cenozoic [*Armijo et al*., 1989], our data require that displacement rates along this system are modest, at least at present [e.g., *Chung et al*., 2008]. Collectively, our results add to the growing perspective that active deformation within the interior of the Tibetan Plateau experiences broadly distributed deformation in response to the ongoing convergence of India with Asia [e.g., *England and Houseman*, 1986] but at relatively slow rates.

5. Conclusions

Displaced lacustrine shorelines developed around Zigui Co in central Tibet place bounds on the Holocene slip rate along the dextral GCF. Our results show that the GCF has accrued 12 ± 2 m of displacement since the deposition of the shorelines at ~4.1–4.4 ka. These results represent the first direct estimate on Holocene slip rate of the GCF of ~2.2–4.5 mm/yr. Modest slip rates along this fault zone are consistent with rates of displacement along other strike-slip faults in central Tibet but are significantly slower than geodetic measures of strain accumulation [*Taylor and Peltzer*, 2006]. Thus, our results both support the notion that active deformation within the interior of the Tibetan Plateau is characterized by slow, distributed deformation and highlight the need for slip rates determined over longer timescales along this and other fault systems in central Tibet.

Acknowledgments

Data to support Figure 4 are available in the supporting information. This work was supported by NSF (EAR-0911587) to E.K. and K.P.F. We thank Kerry Sieh for useful comments on an early version of this paper and Eric Cowgill and Mike Taylor for constructive reviews.

The Editor thanks Michael Taylor and Eric Cowgill for their assistance in evaluating this paper.

References

Ader, T., et al. (2012), Convergence rate across the Nepal Himalaya and interseismic coupling on the Main Himalayan Thrust: Implications for seismic hazard, *J. Geophys. Res.*, *117*, B04403, doi:10.1029/2011JB009071.

Armijo, R., P. Tapponnier, J. L. Mercier, and H. Tong-Lin (1986), Quaternary extension in southern Tibet: Field observations and tectonic implications, *J. Geophys. Res.*, *91*(B14), 13,803–13,872, doi:10.1029/JB091iB14p13803.

Armijo, R., P. Tapponnier, and H. Tonglin (1989), Late Cenozoic right-lateral strike-slip faulting in southern Tibet, *J. Geophys. Res.*, *94*(B3), 2787–2838, doi:10.1029/JB094iB03p02787.

Avouac, J. P., and P. Tapponnier (1993), Kinematic model of active deformation in central Asia, *Geophys. Res. Lett.*, *20*(10), 895–898, doi:10.1029/93GL00128.

Bendick, R., R. Bilham, J. Freymueller, K. Larson, and G. Yin (2000), Geodetic evidence for a low slip rate in the Altyn Tagh fault system, *Nature*, *404*(6773), 69–72.

Bettinelli, P., J.-P. Avouac, M. Flouzat, F. Jouanne, L. Bollinger, P. Willis, and G. Chitrakar (2006), Plate motion of India and interseismic strain in the Nepal Himalaya from GPS and DORIS measurements, *J. Geodesy*, *80*(8-11), 567–589, doi:10.1007/s00190-006-0030-3.

Blisniuk, P. M., and W. D. Sharp (2003), Rates of late Quaternary normal faulting in central Tibet from U-series dating of pedogenic carbonate in displaced fluvial gravel deposits, *Earth Planet. Sci. Lett.*, *215*(1), 169–186.

Brown, E. T., R. Bendick, D. L. Bourlès, V. Gaur, P. Molnar, G. M. Raisbeck, and F. Yiou (2002), Slip rates of the Karakorum Fault, Ladakh, India, determined using cosmic ray exposure dating of debris flows and moraines, *J. Geophys. Res.*, *107*(B9), 2192, doi:10.1029/2000JB000100.

Brown, E. T., P. Molnar, and D. L. Bourlès (2005), Comment on "Slip-rate measurements on the Karakorum Fault may imply secular variations in fault motion", *Science*, *309*(5739), 1326.

Chen, Q., J. T. Freymueller, Q. Wang, Z. Yang, C. Xu, and J. Liu (2004a), A deforming block model for the present-day tectonics of Tibet, *J. Geophys. Res.*, *109*, B01403, doi:10.1029/2002JB002151.

Chen, Q., J. T. Freymueller, Z. Yang, C. Xu, W. Jiang, Q. Wang, and J. Liu (2004b), Spatially variable extension in southern Tibet based on GPS measurements, *J. Geophys. Res.*, *109*, B09401, doi:10.1029/2002JB002350.

Chen, Y., S.-H. Li, and B. Li (2012), Slip rate of the Aksay segment of Altyn Tagh Fault revealed by OSL dating of river terraces, *Quaternary Geochronol.*, *10*, 291–299, doi:10.1016/j.quageo.2012.04.012.

Chen, Y., S.-H. Li, J. Sun, and B. Fu (2013), OSL dating of offset streams across the Altyn Tagh Fault: Channel deflection, loess deposition and implication for the slip rate, *Tectonophysics*, *594*, 182–194, doi:10.1016/j.tecto.2013.04.002.

Chevalier, M.-L., F. J. Ryerson, P. Tapponnier, R. C. Finkel, J. Van Der Woerd, L. Haibing, and L. Qing (2005a), Slip-rate measurements on the Karakorum Fault may imply secular variations in fault motion, *Science*, *307*(5708), 411–414.

Chevalier, M.-L., F. J. Ryerson, P. Tapponnier, R. C. Finkel, J. Van Der Woerd, H. Li, and Q. Liu (2005b), Response to comment on "Slip-rate measurements on the Karakorum Fault may imply secular variations in fault motion," *Science*, *309*(5739), 1326.

Chevalier, M.-L., H. Li, J. Pan, J. Pei, F. Wu, W. Xu, Z. Sun, and D. Liu (2011), Fast slip-rate along the northern end of the Karakorum Fault system, western Tibet, *Geophys. Res. Lett.*, *38*, L22309, doi:10.1029/2011GL049921.

Chevalier, M.-L., P. Tapponnier, J. Van der Woerd, F. J. Ryerson, R. C. Finkel, and H. Li (2012), Spatially constant slip rate along the southern segment of the Karakorum Fault since 200 ka, *Tectonophysics*, *530–531*, 152–179.
Chung, L., Y. Chen, T. Yu, Z. Cao, and G. Yin (2008), New geomorphic evidence for en échelon fault system in East Karakoram-Jiali fault zone, Abstract T53E-2004 presented at 2008 AGU Fall Meeting, San Francisco, Calif., 15–19 Dec.
Cowgill, E. (2007), Impact of riser reconstructions on estimation of secular variation in rates of strike-slip faulting: Revisiting the Cherchen River site along the Altyn Tagh Fault, NW China, *Earth Planet. Sci. Lett.*, *254*(3-4), 239–255.
Cowgill, E., R. D. Gold, C. Xuanhua, W. Xiao-Feng, J. R. Arrowsmith, and J. Southon (2009), Low Quaternary slip rate reconciles geodetic and geologic rates along the Altyn Tagh Fault, northwestern Tibet, *Geology*, *37*(7), 647–650, doi:10.1130/g25623a.1.
Elliott, J. R., J. Biggs, B. Parsons, and T. J. Wright (2008), InSAR slip rate determination on the Altyn Tagh Fault, northern Tibet, in the presence of topographically correlated atmospheric delays, *Geophys. Res. Lett.*, *35*, L12309, doi:10.1029/2008GL033659.
England, P., and G. Houseman (1985), Role of lithospheric strength heterogeneities in the tectonics of Tibet and neighbouring regions, *Nature*, *315*(6017), 297–301.
England, P., and G. Houseman (1986), Finite strain calculations of continental deformation 2. Comparison with the India-Asia collision zone, *J. Geophys. Res.*, *91*(B3), 3664–3676, doi:10.1029/JB091iB03p03664.
Gan, W., P. Zhang, Z.-K. Shen, Z. Niu, M. Wang, Y. Wan, D. Zhou, and J. Cheng (2007), Present-day crustal motion within the Tibetan Plateau inferred from GPS measurements, *J. Geophys. Res.*, *112*, B08416, doi:10.1029/2005JB004120.
Garthwaite, M. C., H. Wang, and T. J. Wright (2013), Broadscale interseismic deformation and fault slip rates in the central Tibetan Plateau observed using InSAR, *J. Geophys. Res. Solid Earth*, *118*, 5071–5083, doi:10.1002/jgrb.50348.
Gold, R. D., E. Cowgill, J. R. Arrowsmith, J. Gosse, X. Chen, and X. Wang (2009), Riser diachroneity, lateral erosion, and uncertainty in rates of strike-slip faulting: A case study from Tuzidun along the Altyn Tagh Fault, NW China, *J. Geophys. Res.*, *114*, B04401, doi:10.1029/2008JB005913.
Harkins, N., and E. Kirby (2008), Fluvial terrace riser degradation and determination of slip rates on strike-slip faults: An example from the Kunlun Fault, China, *Geophys. Res. Lett.*, *35*, L05406, doi:10.1029/2007GL033073.
Harkins, N., E. Kirby, X. Shi, E. Wang, D. Burbank, and F. Chun (2010), Millennial slip rates along the eastern Kunlun Fault: Implications for the dynamics of intracontinental deformation in Asia, *Lithosphere*, *2*(4), 247–266, doi:10.1130/l85.1.
He, J., P. Vernant, J. Chéry, W. Wang, S. Lu, W. Ku, W. Xia, and R. Bilham (2013), Nailing down the slip rate of the Altyn Tagh Fault, *Geophys. Res. Lett.*, *40*, 5382–5386, doi:10.1002/2013GL057497.
Jade, S., B. Bhatt, Z. Yang, R. Bendick, V. Gaur, P. Molnar, M. Anand, and D. Kumar (2004), GPS measurements from the Ladakh Himalaya, India: Preliminary tests of plate-like or continuous deformation in Tibet, *Geol. Soc. Am. Bull.*, *116*(11-12), 1385–1391.
Kirby, E., and N. Harkins (2013), Distributed deformation around the eastern tip of the Kunlun Fault, *Int. J. Earth Sci.*, *102*, 1759–1772.
Kirby, E., N. Harkins, E. Wang, X. Shi, C. Fan, and D. Burbank (2007), Slip rate gradients along the eastern Kunlun Fault, *Tectonics*, *26*, TC2010, doi:10.1029/2006TC002033.
Klinger, Y., M. Etchebes, P. Tapponnier, and C. Narteau (2011), Characteristic slip for five great earthquakes along the Fuyun Fault in China, *Nat. Geosci.*, *4*(6), 389–392.
Li, H., J. Van der Woerd, P. Tapponnier, Y. Klinger, X. Qi, J. Yang, and Y. Zhu (2005), Slip rate on the Kunlun Fault at Hongshui Gou, and recurrence time of great events comparable to the 14/11/2001, Mw∼7.9 Kokoxili earthquake, *Earth Planet. Sci. Lett.*, *237*(1–2), 285–299.
Liang, S., W. Gan, C. Shen, G. Xiao, J. Liu, W. Chen, X. Ding, and D. Zhou (2013), Three-dimensional velocity field of present-day crustal motion of the Tibetan Plateau derived from GPS measurements, *J. Geophys. Res. Solid Earth*, *118*, 5722–5732, doi:10.1002/2013JB010503.
Mériaux, A. S., F. J. Ryerson, P. Tapponnier, J. Van der Woerd, R. C. Finkel, X. Xu, Z. Xu, and M. W. Caffee (2004), Rapid slip along the central Altyn Tagh Fault: Morphochronologic evidence from Cherchen He and Sulamu Tagh, *J. Geophys. Res.*, *109*, B06401, doi:10.1029/2003JB002558.
Molnar, P., and K. E. Dayem (2010), Major intracontinental strike-slip faults and contrasts in lithospheric strength, *Geosphere*, *6*(4), 444–467, doi:10.1130/ges00519.1.
Molnar, P., and H. Lyon-Caen (1989), Fault plane solutions of earthquakes and active tectonics of the Tibetan Plateau and its margins, *Geophys. J. Int.*, *99*(1), 123–153, doi:10.1111/j.1365-246X.1989.tb02020.x.
Murray, A. S., and A. G. Wintle (2000), Luminescence dating of quartz using an improved single-aliquot regenerative-dose protocol, *Radiat. Meas.*, *32*(1), 57–73, doi:10.1016/s1350-4487(99)00253-x.
Paul, J., et al. (2001), The motion and active deformation of India, *Geophys. Res. Lett.*, *28*(4), 647–650, doi:10.1029/2000GL011832.
Peltzer, G., and P. Tapponnier (1988), Formation and evolution of strike-slip faults, rifts, and basins during the India-Asia collision: An experimental approach, *J. Geophys. Res.*, *93*(B12), 15,085–15,117, doi:10.1029/JB093iB12p15085.
Peltzer, G., F. Crampé, and G. King (1999), Evidence of nonlinear elasticity of the crust from the Mw7.6 Manyi (Tibet) earthquake, *Science*, *286*(5438), 272–276, doi:10.1126/science.286.5438.272.
Rittase, W. M., E. Kirby, E. McDonald, J. D. Walker, J. Gosse, J. Q. G. Spencer, and A. J. Herrs (2014), Temporal variations in Holocene slip rate along the central Garlock Fault, Pilot Knob Valley, California, *Lithosphere*, *6*(1), 48–58, doi:10.1130/l286.1.
Rockwell, T. K., S. Lindvall, M. Herzberg, D. Murbach, T. Dawson, and G. Berger (2000), Paleoseismology of the Johnson Valley, Kickapoo, and Homestead Valley Faults: Clustering of earthquakes in the eastern California shear zone, *Bull. Seismol. Soc. Am.*, *90*(5), 1200–1236, doi:10.1785/0119990023.
Shelef, E., and M. Oskin (2010), Deformation processes adjacent to active faults: Examples from eastern California, *J. Geophys. Res.*, *115*, B05308, doi:10.1029/2009JB006289.
Shen, Z. K., M. Wang, Y. Li, D. D. Jackson, A. Yin, D. Dong, and P. Fang (2001), Crustal deformation along the Altyn Tagh Fault system, western China, from GPS, *J. Geophys. Res.*, *106*(B12), 30,607–30,621, doi:10.1029/2001JB000349.
Stirling, M., D. Rhoades, and K. Berryman (2002), Comparison of earthquake scaling relations derived from data of the instrumental and preinstrumental era, *Bull. Seismol. Soc. Am.*, *92*(2), 812–830, doi:10.1785/0120000221.
Taylor, M., and G. Peltzer (2006), Current slip rates on conjugate strike-slip faults in central Tibet using synthetic aperture radar interferometry, *J. Geophys. Res.*, *111*, B12402, doi:10.1029/2005JB004014.
Taylor, M., and A. Yin (2009), Active structures of the Himalayan-Tibetan orogen and their relationships to earthquake distribution, contemporary strain field, and Cenozoic volcanism, *Geosphere*, *5*(3), 199–214, doi:10.1130/ges00217.1.
Taylor, M., A. Yin, F. J. Ryerson, P. Kapp, and L. Ding (2003), Conjugate strike-slip faulting along the Bangong-Nujiang suture zone accommodates coeval east-west extension and north-south shortening in the interior of the Tibetan Plateau, *Tectonics*, *22*(4), 1044, doi:10.1029/2002TC001361.
Van der Woerd, J., F. J. Ryerson, P. Tapponnier, Y. Gaudemer, R. Finkel, A. S. Meriaux, M. Caffee, Z. Guoguang, and H. Qunlu (1998), Holocene left-slip rate determined by cosmogenic surface dating on the Xidatan segment of the Kunlun Fault (Qinghai, China), *Geology*, *26*(8), 695–698, doi:10.1130/0091-7613(1998)026<0695:hlsrdb>2.3.co;2.

Van der Woerd, J., F. J. Ryerson, P. Tapponnier, A. S. Meriaux, Y. Gaudemer, B. Meyer, R. C. Finkel, M. W. Caffee, Z. Guoguang, and X. Zhiqin (2000), Uniform slip-rate along the Kunlun Fault: Implications for seismic behaviour and large-scale tectonics, *Geophys. Res. Lett.*, *27*(16), 2353–2356, doi:10.1029/1999GL011292.

Van Der Woerd, J., P. Tapponnier, F. J. Ryerson, A. S. Meriaux, B. Meyer, Y. Gaudemer, R. C. Finkel, M. W. Caffee, G. G. Zhao, and Z. Q. Xu (2002), Uniform postglacial slip-rate along the central 600 km of the Kunlun Fault (Tibet), from Al-26, Be-10, and C-14 dating of riser offsets, and climatic origin of the regional morphology, *Geophys. J. Int.*, *148*(3), 356–388.

Wallace, R. E. (1987), Grouping and migration of surface faulting and variations in slip rates on faults in the Great Basin province, *Bull. Seismol. Soc. Am.*, *77*(3), 868–876.

Wang, Q., et al. (2001), Present-day crustal deformation in China constrained by Global Positioning System measurements, *Science*, *294*(5542), 574–577.

Washburn, Z., J. R. Arrowsmith, S. L. Forman, E. Cowgill, W. Xiaofeng, Z. Yueqiao, and C. Zhengle (2001), Late Holocene earthquake history of the central Altyn Tagh Fault, China, *Geology*, *29*(11), 1051–1054.

Wright, T. J., B. Parsons, P. C. England, and E. J. Fielding (2004), InSAR observations of low slip rates on the major faults of western Tibet, *Science*, *305*(5681), 236–239.

Wu, Z., Z. Cao, B. Shetu, and Q. D. Deng (1990), Surface ruptures by earthquake found in Xainza, central Xizang [in Chinese with English abstract], *Seismol. Geol.*, *12*(4), 317–319.

Xu, X., G. Yu, Y. Klinger, P. Tapponnier, and J. Van Der Woerd (2006), Reevaluation of surface rupture parameters and faulting segmentation of the 2001 Kunlunshan earthquake (Mw7.8), northern Tibetan Plateau, China, *J. Geophys. Res.*, *111*, B05316, doi:10.1029/2004JB003488.

Yin, A., and M. H. Taylor (2011), Mechanics of V-shaped conjugate strike-slip faults and the corresponding continuum mode of continental deformation, *Geol. Soc. Am. Bull.*, *123*(9–10), 1798–1821.

Yin, A., P. A. Kapp, M. A. Murphy, C. E. Manning, T. Mark Harrison, M. Grove, D. Lin, D. Xi-Guang, and W. Cun-Ming (1999), Significant late Neogene east-west extension in northern Tibet, *Geology*, *27*(9), 787–790, doi:10.1130/0091-7613(1999)027<0787:slnewe>2.3.co;2.

Zhang, P., Z. Shen, M. Wang, W. Gan, R. Burgmann, P. Molnar, Q. Wang, Z. Niu, J. Sun, and J. Wu (2004), Continuous deformation of the Tibetan Plateau from Global Positioning System data, *Geology*, *32*(9), 809–812.

Zhang, P., P. Molnar, and X. Xu (2007), Late Quaternary and present-day rates of slip along the Altyn Tagh Fault, northern margin of the Tibetan Plateau, *Tectonics*, *26*, TC5010, doi:10.1029/2006TC002014.

Zielke, O., J. R. Arrowsmith, L. G. Ludwig, and S. O. Akçiz (2010), Slip in the 1857 and earlier large earthquakes along the Carrizo Plain, San Andreas Fault, *Science*, *327*(5969), 1119–1122, doi:10.1126/science.1182781.